Preparation of Activated Carbons from Hemicellulose Pre-Extraction Residue of Eucalyptus Heartwood and Sapwood and their Application in Toluene Adsorption

Xixiang Huang,[a,b] Yuanyuan Zhao,[b,c] Zhiwei Wang,[b] Yanhong Wang,[c] Yun Zhou,[c] Hao Cheng,[a] Penghui Li,[a] and Shubin Wu [a,*]

**Corresponding author: Shubinwu@scut.edu.cn*

DOI: 10.15376/biores.20.1.2259-2275

GRAPHICAL ABSTRACT

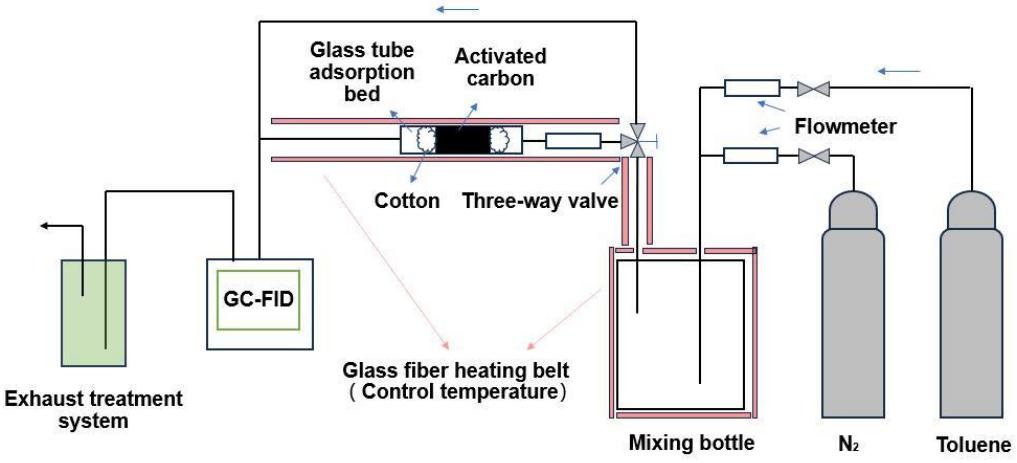

Preparation of Activated Carbons from Hemicellulose Pre-Extraction Residue of Eucalyptus Heartwood and Sapwood and their Application in Toluene Adsorption

Xixiang Huang,[a,b] Yuanyuan Zhao,[b,c] Zhiwei Wang,[b] Yanhong Wang,[c] Yun Zhou,[c] Hao Cheng,[a] Penghui Li,[a] and Shubin Wu [a,*]

Pre-extraction of hemicellulose from eucalyptus heartwood and sapwood was conducted using the method of KOH extraction. Activated carbons (ACs) with high toluene adsorption capacity were prepared by using KOH as activator and hemicellulose-pre-extracted residue (HPR) as AC precursor. The findings indicated that the pore structure of the ACs could be regulated by adjusting the carbonization temperature. Using the HPR of eucalyptus heartwood as raw material, the activated carbon carbonized at 400 °C exhibited the highest BET surface area (3699 $m^2 \cdot g^{-1}$) and pore volume (1.90 $cm^3 \cdot g^{-1}$). The adsorption capacity of AC for toluene reached 816 $mg \cdot g^{-1}$. The results showed that the adsorption capacity of toluene was associated with the micropores (< 2 nm) in the AC. Optimizing the carbonization temperature could enhance the proportion of micropores, thereby significantly enhancing the activated carbon's adsorption capacity for toluene.

DOI: 10.15376/biores.20.1.2259-2275

Keywords: Eucalyptus heartwood; Eucalyptus sapwood; Carbonization temperature; Activated carbon; Toluene adsorption

Contact information: a: State Key Laboratory of Pulp and Paper Engineering, South China University of Technology, Guangzhou 510540, P.R. China; b: Key Laboratory of Clean Pulp and Papermaking and Pollution Control of Guangxi, College of Light Industry and Food Engineering, Guangxi University, Nanning 530004, P.R. China; c: Guanghou Paper Group Ltd, Guangzhou 511462, P.R. China;
** Corresponding author: Shubinwu@scut.edu.cn*

INTRODUCTION

With the rapid advancement of the global economy, unregulated use and excessive consumption of petroleum fuels have aggravated the pollution and destruction of the ecological environment, and the atmospheric pollution problem represented by the global greenhouse effect and volatile organic compounds (VOCs) has become an urgent global problem to be solved. VOCs refer to organic compounds with saturated vapor pressure higher than 133.3 Pa and boiling point between 50 and 260 °C at ambient pressure. VOCs are extremely harmful atmospheric pollutants, serving as not only precursors to haze but also being capable of reacting with nitrogen oxides to form photochemical smog, leading to the depletion of the ozone layer and causing significant damage to the ecological environment. The majority of VOCs exhibit strong irritant and toxic properties, while some also possess carcinogenic, teratogenic, mutagenic, and other characteristics that pose substantial risks to human health (David *et al.* 2021). There are many techniques to remove VOCs, such as catalytic oxidation, photocatalytic oxidation, reverse osmosis, ion exchange, thermal oxidation, biological treatment, and adsorption (Wu *et al.* 2023).

Among them, the adsorption method is the simplest, most efficient, and economical method because of stable operation, no toxic by-products and low cost (Wen *et al*. 2023). Activated carbon, as a type of carbon material characterized by its wide range of sources, exceptional pore structure, and high adsorption capacity, finds extensive application in the adsorption and separation of VOCs gas.

Coal has traditionally been a primary raw material for the production of activated carbon. However, growing concerns over environmental pollution and energy scarcity have led to an increased emphasis on renewable resources as substitutes for fossil-based materials. Plant raw materials have become important materials for the preparation of activated carbon because of their wide source and renewable use. A series of studies have been conducted to produce activated carbon from various plant fiber materials, such as wood (Zuo *et al.* 2023), straw (Yang *et al.* 2021), fruit husks (Sathya *et al.* 2019), bark (Sessa *et al.* 2022), branches (Li *et al.* 2024), lignin (Li *et al*. 2023), bamboo (Yang *et al.* 2023), and bagasse (Qin *et al.* 2019). The eucalyptus tree is a strategically important species in China due to its rapid growth and strong adaptability (Murata *et al.* 2021). It is extensively cultivated and utilized in the southern regions of China, playing a key role in modern artificial afforestation efforts. The sapwood layer of eucalyptus is relatively broad and presents as white to light pink. It features a relatively loose cell structure, lower density, softer material, and a relatively rapid drying speed. Meanwhile, the heartwood is light reddish-brown. It has a longer growth period, a more compact cell structure, higher density, and greater strength. Eucalyptus raw materials or industrial scraps are abundant in cellulose, hemicellulose, and lignin, which play a crucial role in the high-value conversion of biomass resources. Hemicellulose, characterized by its amorphous structure and low molecular weight, exhibits the lowest thermal stability among the three components. It initiates decomposition at 220 °C and is prone to thermal degradation, leading to its limited contribution to carbon quality. Throughout the carbon production processes, a significant portion of it undergoes transformation into volatile components such as CO, CO_2, and CH_4 (Zhang *et al.* 2017). Therefore, pre-extracting hemicellulose from eucalyptus raw materials to make composite materials such as hydrogels, aerogels, drug carriers, and sensors could achieve high-value applications while mitigating the inefficiency due to loss of hemicellulose during biomass carbonization.

The preparation process of activated carbon actually converts organic matter into a volatile form at high temperatures through thermal decomposition and thermal polymerization, thus consuming non-carbon components and generating a large number of microporous structures. This process includes decomposition reactions and polycondensation reactions, and is directly affected by factors such as temperature, time, heating rate and protective airflow velocity. Among them, carbonization temperature has great influence on activated carbon adsorption. This is because the carbonization temperature directly affects the reaction process of activated carbon. With the change of temperature, the reaction rate of carbon in activated carbon raw materials also changes, resulting in differences in the specific surface area and total pore volume of activated carbon, and the adsorption performance changes. When the carbonization temperature exceeds a certain threshold, the reaction rate accelerates excessively, leading to the occurrence of micropore burning loss and subsequent 'peeling' reactions. This results in a rapid reduction in both specific surface area and pore volume of activated carbon, consequently diminishing its adsorption performance (Hassan *et al.* 2014). By utilizing corn cob as a carbon precursor, Zhu *et al*. (2018) investigated the impact of carbonization conditions on the production of activated carbon (Zhu *et al*. 2018). They successfully

obtained an optimal carbon material with a specific surface area of 2022 $m^2 \cdot g^{-1}$ and an adsorption capacity for toluene of 415 $mg \cdot g^{-1}$. Xie *et al.* (2022) prepared activated carbon from prickly ash branches, studied the effect of hydrothermal pretreatment temperature on the structure and chemical properties of activated carbon, and prepared activated carbon with specific surface area of 1291 $m^2 \cdot g^{-1}$ and toluene adsorption capacity of 533 $mg \cdot g^{-1}$ (Xie *et al.* 2022). By modifying the conditions of alkali extraction, He *et al.* (2023) investigated the impact of hemicellulose removal degree on the pore structure of poplar-based activated carbon. They achieved the optimal carbon material with a specific surface area of 3066 $m^2 \cdot g^{-1}$ and an adsorption capacity for toluene of 733 $mg \cdot g^{-1}$ (He *et al*. 2023).

In this study, hemicellulose was pre-extracted from eucalyptus heartwood and sapwood using KOH at 85 ℃. ACs with high toluene adsorption capacity were prepared by using KOH as activator and extraction residue as carbon precursor, achieving high conversion and utilization of hemicellulose. Firstly, the impact of carbonization temperature on the yield and pore structure of activated carbon was investigated. Then, the influence of eucalyptus heartwood and sapwood on hemicellulose pre-extraction and activated carbon preparation was assessed. Finally, toluene, a typical component of VOCs, was chosen to assess the adsorption performance of activated carbon, investigating the relationship between the adsorption capacity and micropores.

EXPERIMENTAL

Materials

The eucalyptus heartwood and sapwood utilized in the experiment were collected from a wood-based panel company located in Guangdong Province. Benzene, potassium hydroxide, hydrochloric acid and anhydrous ethanol were procured from the Guangzhou Chemical Reagent Factory. Dry air (99.999% purity) and argon (99.999% purity) were obtained from Guangzhou Shengying Gas Co., Ltd. The 500 ppm toluene and nitrogen standard gas was acquired from Foshan Kede Gas Chemical Co., Ltd.

Preparation of Carbon Precursors

The eucalyptus heartwood and sapwood were air-dried, pulverized, then filtered through a 40- to 60-mesh sieve and subsequently dried at 105 °C. Eucalyptus heartwood powder and eucalyptus sapwood powder were extracted for 6 h using a benzene-ethanol mixture (2:1, v:v), followed by air drying at 105 ℃ for 24 h. The resulting raw materials after extraction were labeled as Eh and Es, respectively. The GB/T 35818-2018 (Chinese National Standard) describes in detail the pre-extraction process of organic solvents. The Eh and Es were treated with a 10 wt% KOH solution at 85 ℃, a solid-liquid ratio of 1:20 (g:mL) for 3 h. Hemicellulose solution (filtrate) and solid residue were obtained through solid-liquid separation. The hemicellulose pre-extracted residue (HPR) was rinsed with water to achieve neutral pH and then dried for 24 h at 105 °C, resulting in samples labeled EhHPR and EsHPR, respectively.

Analysis of Carbon Precursor Compositions

The GB/T 35818 (2018) standard provides detailed guidelines for determining the content of holocellulose and Klason lignin. The determination of α-cellulose content is outlined in GB/T 744 (2004), which involves treating delignified raw materials with a 17.5% sodium hydroxide solution. Hemicellulose content is expressed by subtracting the

difference of the α-cellulose content from the holocellulose content. Organic solvent extract content involves extraction using a benzene-ethanol mixture, while ash content is determined by incinerating samples in a muffle furnace at 575 ℃, following the specific procedures outlined in GB/T 35818 (2018).

Preparation of Activated Carbons

A total of 2 g of EhHPR or EsHPR were placed into an alumina sample boat and moved it into a tube furnace, then heated to a temperature range of 300 to 500 ℃ at a controlled heating rate of 10 ℃·min^{-1} under argon gas with a flow rate of 300 mL·min^{-1}, and maintained at this temperature for an hour. Subsequently, the sample was naturally cooled to room temperature to obtain the carbonized solid. The resulting carbonized solid was mixed with KOH in an exact mass ratio of 1:5 (measured by dry weight), followed by addition to ultra-pure water while stirring thoroughly. The mixture was then dried in an oven at 105 ℃ for 24 h before being transferred into a porcelain crucible. Finally, the sample was subjected to temperature activation under argon gas flowing at a rate of 300 mL·min^{-1}, reaching up to 800 ℃ at a controlled heating rate of 10 ℃·min^{-1} and maintaining this temperature for another hour. After being cooled to room temperature, the resulting ACs underwent an HCl wash, followed by a rinse with ultra-pure water until reaching neutral pH. The sample was dried in a 105 ℃ drying oven for 24 h, and ACs were obtained and stored in a sealed vial. The ACs produced from EhHPR were labeled as EhHPC. Similarly, the ACs produced from EsHPR were labeled as EsHPC. As a control, the ACs produced from Eh and Es without hemicellulose pre-extracted were labeled as EhC and EsC, respectively. The ACs produced from EhHPR at different carbonization temperatures were labeled as EhHPC-300, EhHPC-350, EhHPC-400, EhHPC-450, and EhHPC-500, respectively. Similarly, the ACs produced from EsHPR at different carbonization temperatures were labeled as EsHPC-300, EsHPC-350, EsHPC-400, EsHPC-450 and EsHPC-500, respectively.

Characterization of Activated Carbons

Specific surface area and pore structure analysis

The experiment used a pore structure analyzer ASAP 2460 to measure the N_2 adsorption/desorption isotherms of ACs at 77 K and calculate the pore structure parameters. Samples were degassed at 300 ℃ for 10 h before testing to remove moisture and impurities inside the sample, and the sample weight was not less than 50 mg during testing. The specific surface area (S_{BET}) of sample was calculated by BET (Brunauer-Emmett-Teller) equation. The total pore volume (V_{total}) was obtained from the adsorption capacity of N_2 at the relative pressure P/P_0=0.95. Micropore specific surface area (S_{micro}) and micropore volume (V_{micro}) were calculated by Density Functional Theory (DFT). Mesoporous specific surface area (S_{meso}) and mesoporous volume (V_{meso}) were calculated by BJH (Barrett-Joyner-Halenda) method. Pore size distribution (PSD) of AC was obtained by DFT model.

Scanning electron microscope (SEM) analysis

The samples were subjected to analysis of their microscopic morphology and pore structure using a scanning electron microscope. A trace amount of dry activated carbon powder was directly glued to the conductive adhesive, and gold spraying was carried out. The morphology of the sample was photographed with a TESCAN MIRA LMS scanning electron microscope, and the accelerated voltage was 3 kV.

Dynamic Adsorption Test of Toluene

As shown in Fig. 1, the dynamic adsorption device was connected, and then the adsorption amount of toluene was measured. Prior to the adsorption test, the activated carbon sample underwent degassing in a vacuum drying oven at 100 °C for 10 h to eliminate moisture content. High purity nitrogen was then utilized to purge the air and residual toluene gas from the testing system. The experimental conditions for dynamic toluene adsorption were set as follows: activated carbon mass: 0.100 g (± 1%); gas flow rate: 200 mL·min^{-1}; toluene concentration: 500 ppm; temperature: 30 °C; adsorption bed: glass tube with an inner diameter of 5 mm and a length of 160 mm; testing instrument: Gas chromatograph GC2002 (Shanghai Kechuang). To minimize the impact of systematic error on adsorption capacity, the blank adsorption capacity was determined by measuring the adsorption breakthrough curve in the absence of samples. Subsequently, the actual adsorption capacity of the sample was calculated as the difference between total capacity and blank adsorption capacity. The relationship between adsorption capacity (Q) and time (t) was calculated using Eq. 1,

$$Q = \frac{V}{m} C_0 (t - \int_0^t C_t / C_0 dt) \times 10^{-6} \quad (1)$$

where V is the toluene gas flow rate (mL·min^{-1}), m is the sample mass (g), Q is the adsorption capacity (mg·g^{-1}), C_0 is the inlet concentration of toluene gas (g·m^{-3}), C_t is the outlet concentration of toluene gas (g·m^{-3}) at t (min), and t is the adsorption time (min).

The penetration time t_b is the time when C_t/C_0 is 5%, the saturation time t_s is the time when C_t/C_0 is 95%, the penetration adsorption quantity Q_b corresponds to the adsorption quantity at t_b moment, and the saturation adsorption quantity Q_s corresponds to the adsorption quantity at t_s moment.

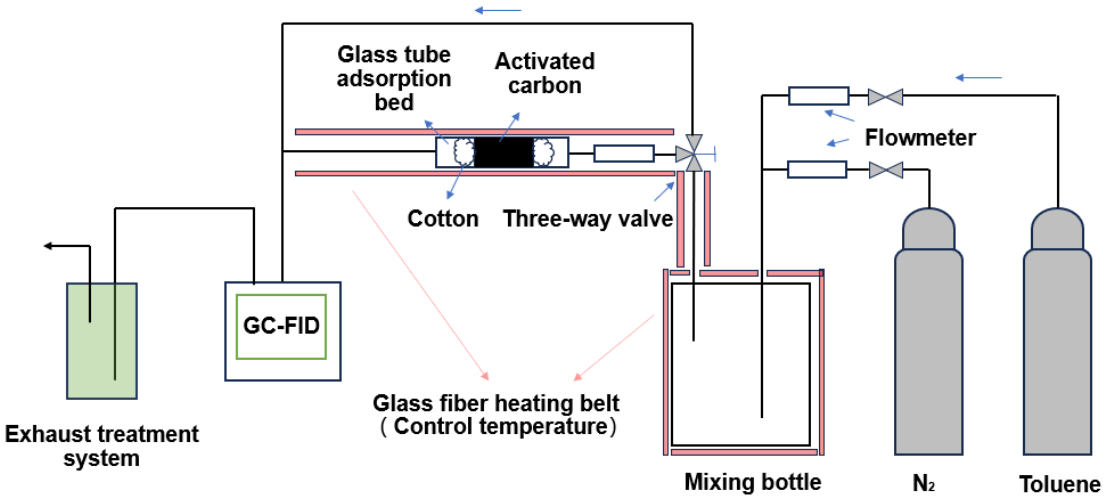

Fig. 1. Dynamic adsorption device for toluene

The Yoon-Nelson (Y-N) model (Yoon and Nelson 1984) is a semi-empirical approach used for nonlinear fitting of adsorption permeation curves, as shown in Eq. 2,

$$\ln \frac{C_t}{C_0 - C_t} = K_{YN} t - \tau K_{YN} \quad (2)$$

where C_t is the outlet concentration of toluene gas at t (min), C_0 is the inlet concentration

of toluene gas ($g \cdot m^{-3}$), K_{YN} is the adsorption rate constant (min^{-1}), t is the adsorption time (min), and τ is the time for 50% of the adsorbate to penetrate through the adsorbent fixed bed (min). This equation can be utilized to determine the adsorption rate and the penetration time of adsorbing 50 percent toluene.

RESULTS AND DISCUSSION

Effect of Carbonization Temperature on Pore Characteristics and Adsorption Performance of EhHPC and EsHPC

The N_2 adsorption/desorption isotherms of EhHPC and EsHPC at different carbonization temperatures were depicted in Fig. 2 (a) and (b). All isotherms exhibited typical type I behavior, indicating that the prepared activated carbon possessed a significant number of micropores. When the carbonization temperature ranged from 300 to 500 ℃, the adsorption capacity of EhHPC and EsHPC initially increased and then decreased, reaching its peak at 400 ℃. The adsorption capacity of EhHPC-400 exceeded that of EsHPC-400.

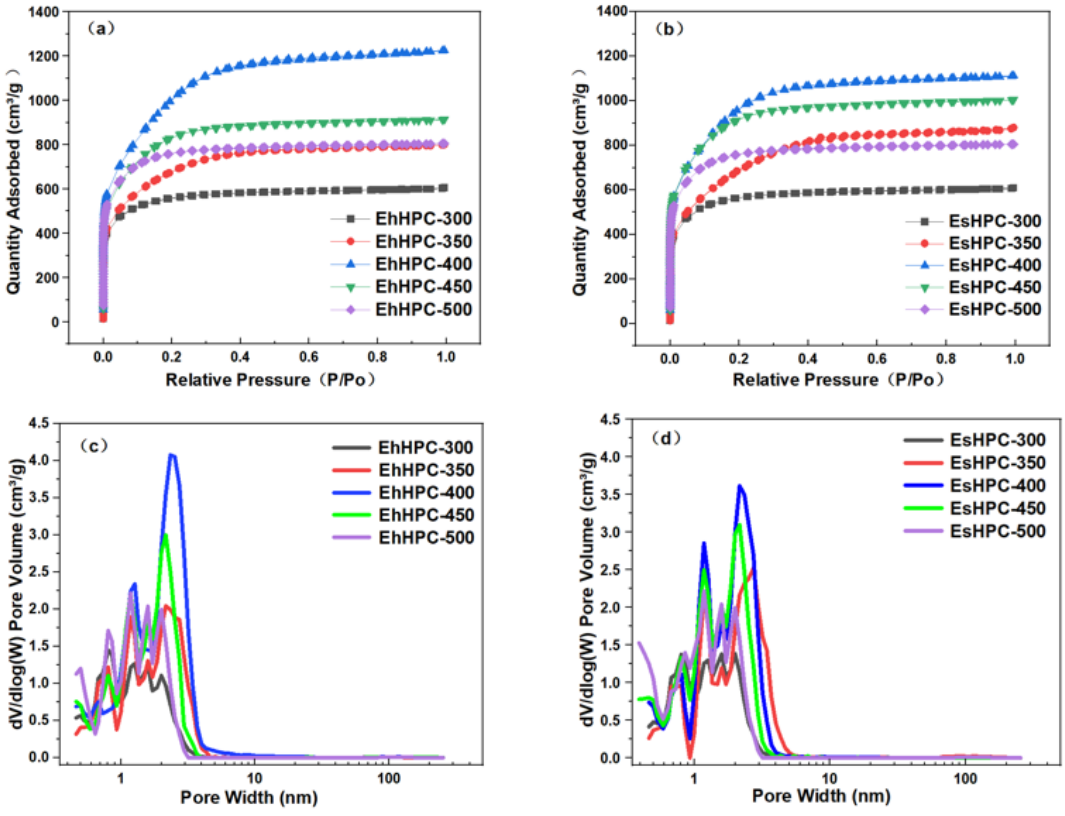

Fig. 2. N_2 adsorption/desorption isotherms (a, b) and pore size distributions (c,d) of EhHPC and EsHPC at different carbonization temperatures

The pore size distributions of EhHPC and EsHPC are shown in Fig. 2(c) and (d), respectively, indicating that the pores in the prepared ACs consisted mainly of micropores and mesoporous pores. Both EhHPC and EsHPC exhibited a trend of increasing then decreasing micropores and mesopores, reaching an optimum at 400 ℃. EhHPC-400 in

Fig. 2(c) and EsHPC-400 in Fig. 2(d) indicated that the multistage pore structures of the two carbon materials were mainly concentrated in micropores below 2 nm and mesoporous pores between 2 nm and 4 nm, with significant peaks around 1.5 nm and 2.5 nm; however, the peak value at about 2.5 nm was higher for EhHPC-400 compared to EsHPC-400.

Table 1. Pore Performance Parameters of EhHPC at Different Carbonization Temperatures

Sample	[a]S_{BET} ($m^2 \cdot g^{-1}$)	[b]S_{micro} ($m^2 \cdot g^{-1}$)	[c]S_{meso} ($m^2 \cdot g^{-1}$)	[d]V_{total} ($cm^3 \cdot g^{-1}$)	[b]V_{micro} ($cm^3 \cdot g^{-1}$)	[c]V_{meso} ($cm^3 \cdot g^{-1}$)	[e]D_P (nm)
EhHPC-300	2087	1959	97	0.93	0.82	0.09	1.79
EhHPC-350	2455	2217	138	1.23	1.04	0.18	2.02
EhHPC-400	3699	3175	274	1.90	1.48	0.40	2.05
EhHPC-450	3094	2692	192	1.41	1.14	0.27	1.82
EhHPC-500	2877	2726	105	1.24	1.12	0.10	1.73

Table 2. Pore Performance Parameters of EsHPC at Different Carbonization Temperatures

Sample	[a]S_{BET} ($m^2 \cdot g^{-1}$)	[b]S_{micro} ($m^2 \cdot g^{-1}$)	[c]S_{meso} ($m^2 \cdot g^{-1}$)	[d]V_{total} ($cm^3 \cdot g^{-1}$)	[b]V_{micro} ($cm^3 \cdot g^{-1}$)	[c]V_{meso} ($cm^3 \cdot g^{-1}$)	[e]D_P (nm)
EsHPC-300	2131	2009	101	0.94	0.83	0.11	1.76
EsHPC-350	2500	2257	162	1.36	1.13	0.23	2.17
EsHPC-400	3553	3161	202	1.72	1.42	0.29	1.93
EsHPC-450	3397	3134	147	1.55	1.35	0.20	1.82
EsHPC-500	2823	2683	93	1.18	1.09	0.08	1.67

a: S_{BET} is the specific surface area; b: S_{micro} and V_{micro} are the specific surface area and volume of micropores; c: S_{meso} and V_{meso} are mesoporous specific surface areas and mesoporous volume; d: V_{total} is the total pore volume; e: D_p is the average aperture.

To gain a deeper insight into the pore structure of the activated carbon samples, Table 1 and Fig. 2a show the main calculated pore structure parameters of EhHPC, along with presenting the variations in these parameters in Fig. 3(a) and (c). Similarly, Table 2 lists the main pore structure parameters of EsHPC calculated in Fig. 2(b) and (d), while their changes are depicted in Figs. 3(b) and (d). Table 1 and Fig. 3(a) and (c) illustrate that within the carbonization temperature range of 300 to 500 ℃, S_{BET}, S_{micro}, S_{meso}, V_{total}, V_{micro}, and V_{meso} of EsHPC exhibited an initial increase followed by a decrease with rising temperature, reaching their peak values at 400 ℃. Similarly, Table 2 and Fig. 3(b) and (d) demonstrated that S_{BET}, S_{micro}, S_{meso}, V_{total}, V_{micro}, and V_{meso} of EsHPC also followed a similar trend with maximum values observed at 400 ℃. Among the 10 samples tested, EsHPC-400 displayed the highest BET specific surface area (3699 $m^2 \cdot g^{-1}$) and pore volume (1.90 $cm^3 \cdot g^{-1}$). Based on the analysis of Table 1, Table 2, and Fig. 3, ACs from HPR of eucalyptus heartwood and sapwood exhibited a significant impact from the carbonization temperature within the range of 300 to 400 ℃. An increase in carbonization temperature promoted the transition from micropores to mesoporous pores and facilitated the formation of more micropores. However, further increase the carbonization temperature (from 400 to 500 ℃) may lead to pore structure collapse, resulting in decreased specific surface area and total pore volume of activated carbon. Therefore, selecting an appropriate carbonization temperature was crucial. In this study, the optimum carbonization temperature was 400 ℃.

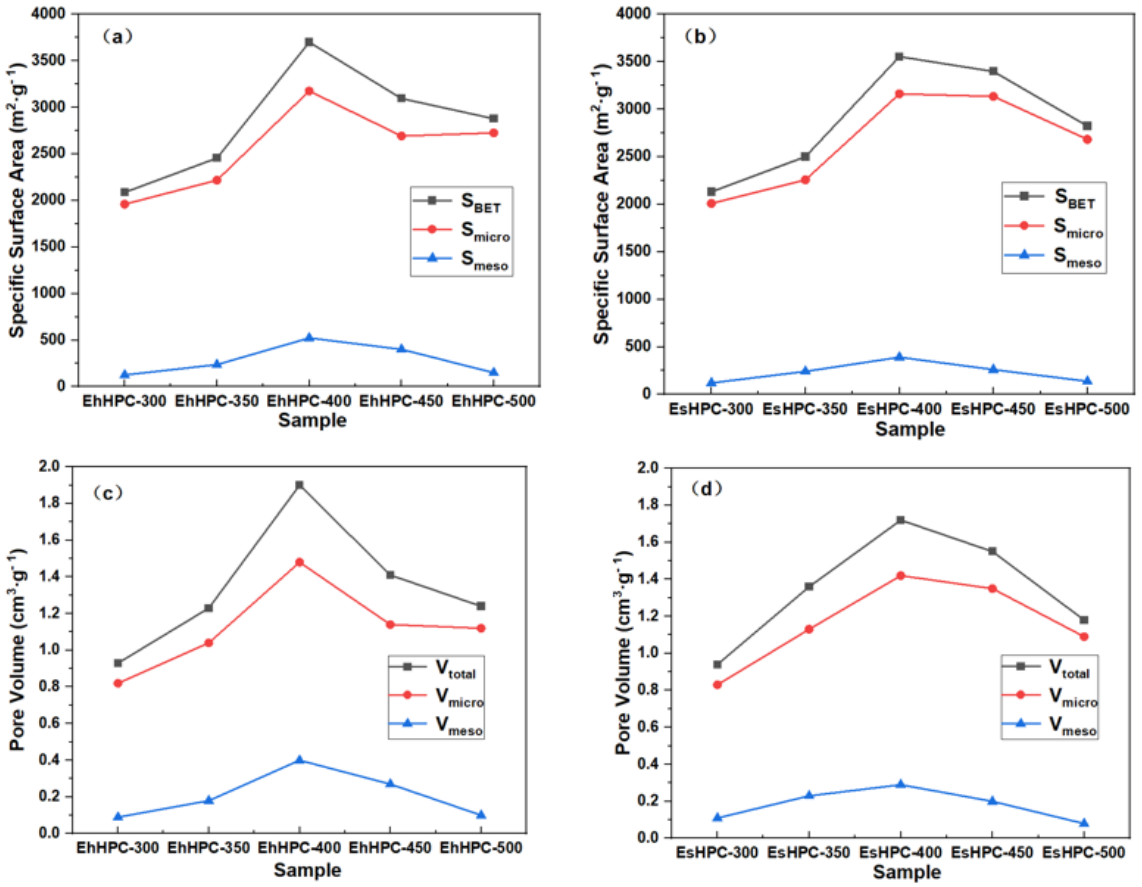

Fig. 3. Specific surface area change image (a, b), and pore volume change image (c, d) of EhHPC and EsHPC at different carbonization temperatures

Effect of Pre-extraction of Hemicellulose on the Pore Characteristics and the Adsorption Ability for Toluene of ACs

To illustrate the effect of pre-extraction of hemicellulose on the pore characteristics, the N_2 adsorption/desorption isotherms and pore size distributions of EhC-400, EsC-400, EhHPC-400, and EsHPC-400 are depicted in Fig. 4 (a) and (b). In Fig. 4 (a), the N_2 adsorption/desorption isotherms of EhC-400 and EsC-400 were almost the same. The N_2 adsorption/desorption isotherms of EhHPC-400 and EsHPC-400 were higher than that of EhC-400 and EsC-400, respectively. This indicated that pre-extraction of hemicellulose was beneficial for increasing adsorption capacity for ACs. In Fig. 4 (b), the pore volume of EhHPC-400 and EsHPC-400 was lower at about 0.5 nm than that of EhC-400 and EsC-400, but higher at about 1.5 nm and 2.5 nm than that of EhC-400 and EsC-400. This may indicate that the pre-extraction of hemicellulose was beneficial for the conversion of micropores around 0.5 nm to micropores around 1.5 and 2.5 nm, as well as the formation of more micropores. Table 3 listed the main pore structure parameters of EhC-400, EsC-400, EhHPC-400 and EsHPC-400. It could be analyzed that after pre-extraction of hemicellulose, S_{BET}, S_{micro}, S_{meso}, V_{micro}, V_{meso}, and D_P all showed an increasing trend, with S_{micro} and V_{micro} showing the largest growth values. This indicated that pre-extraction of hemicellulose for the production of ACs was beneficial for increasing specific surface area and pore volume, especially for micropores. It also explained the reasons for the increase in adsorption capacity in Fig. 4 (a) and pore volume in Fig. 4 (b).

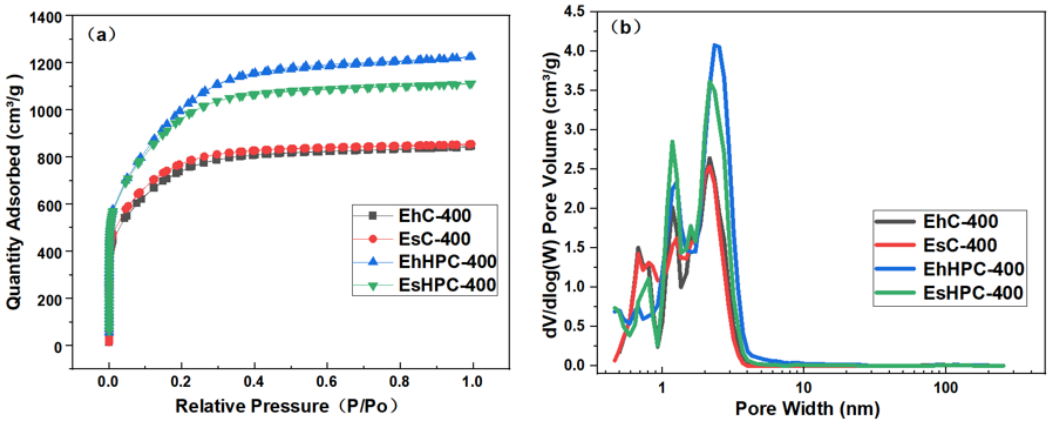

Fig. 4. N_2 adsorption/desorption isotherms (a), and pore size distributions (b) of EhC-400, EsC-400, EhHPC-400 and EsHPC-400

Table 3. Pore Performance Parameters of EhC-400, EsC-400, EhHPC-400 and EsHPC-400

Sample	[a]S_{BET} ($m^2 \cdot g^{-1}$)	[b]S_{micro} ($m^2 \cdot g^{-1}$)	[c]S_{meso} ($m^2 \cdot g^{-1}$)	[d]V_{total} ($cm^3 \cdot g^{-1}$)	[b]V_{micro} ($cm^3 \cdot g^{-1}$)	[c]V_{meso} ($cm^3 \cdot g^{-1}$)	[e]D_P (nm)
EhC-400	2713	2539	173	1.31	1.12	0.19	1.92
EsC-400	2863	2571	178	1.32	1.15	0.17	1.84
EhHPC-400	3699	3175	274	1.90	1.48	0.40	2.05
EsHPC-400	3553	3161	202	1.72	1.42	0.29	1.93

a: S_{BET} is the specific surface area; b: S_{micro} and V_{micro} are the specific surface area and volume of micropores; c: S_{meso} and V_{meso} are mesoporous specific surface areas and mesoporous volume; d: V_{total} is the total pore volume; e: D_p is the average aperture.

Table 4. Composition Analysis of Eh, Es and EhHPR, EsHPR

Sample	Holocellulose (%)	α-Cellulose (%)	Hemicellulose (%)	Klason-lignin (%)	Organic Extractives (%)
Eh	73.6	41.3	32.3	25.5	0.6
Es	78.7	47.9	30.8	21.2	0.2
EhHPR	67.5	54.1	13.4	32.5	—
EsHPR	65.9	54.7	11.2	34.1	—

Table 4 lists the holocellulose, α-cellulose, hemicellulose, and Klason-lignin contents in Eh, Es, EhHPR, and EsHPR. The hemicellulose and Klason-lignin content of Eh were high than that of Es. The α-cellulose content in Es (eucalyptus sapwood) reached 47.9%, with a low Klason-lignin content of 21.2%. After 10% KOH extraction to removal most of hemicellulose, the hemicellulose content decreased from 32.3% to 13.4% for Ec. Although the hemicellulose content of Eh was higher than that of Es, the hemicellulose content of EsHPR was reduced to 11.2% after being treated with 10% KOH at 85 °C, which was lower than the hemicellulose content of EhHPR. This was because the cell wall of eucalyptus heartwood was relatively thick, and the hemicellulose removal was not as easy as Es under the same KOH extraction condition. Analysis of Table 4 revealed that the hemicellulose content exhibited the most significant changes following KOH extraction. Combined with the data in Fig. 4 and Table 3, it could be concluded that pre-extraction of hemicellulose could generate more micropores in ACs, thereby increasing its adsorption capacity and pore volume.

Morphological Analysis of EhC-400, EsC-400, EhHPC-400 and EsHPC-400

The morphologies of EhC-400(a, b), EsC-400(c, d), EhHPC-400(e, f), and EsHPC-400(g, h) were characterized by SEM, and the results are shown in Fig. 5. All ACs had similar microstructures, composed of irregular particles with irregular pores, and exhibited the result of activator erosion and pore formation. However, with the pre-extraction of hemicellulose, the ACs showed more abundant pores, as shown in Fig. 5 EhHPC-400 (e, f) and EsHPC-400 (g, h). It was speculated that the possible reason was the formation of more channels in the plant fiber structure during the pre-extraction of hemicellulose, which provided more reaction space and exacerbates the erosive effect of KOH, resulting in higher specific surface area and pore volume. Figure 5 EhHPC-400 (e, f) and EsHPC-400 (g, h) revealed that the holes in AC from EsHPC-400 were smoother than those from EhHPC-400. This may be because the cell structure of the sapwood was relatively loose, while the heartwood grows in the center of the tree, with higher strength and hardness than the sapwood. After the pre-extraction of hemicellulose, KOH was more likely to corrode the sapwood, forming smoother pores. However, the specific surface area and pore volume of EhHPC-400 were higher than those of EsHPC-400 (see Table 3), suggesting that it may be due to hardness and strength reasons. Some pores that should have formed in EsHPC-400 collapsed, resulting in the loss of pore structure. That is to say, the strength and hardness of the fiber raw materials themselves may have a certain impact on the preparation of ACs.

Analysis of Toluene Adsorption Properties of ACs

To investigate the toluene adsorption capacity of different ACs, dynamic adsorption experiments were conducted (EhC-400, EhHPC-300, EhHPC-350, EhHPC-400, EhHPC-450, EhHPC-500, EsC-400, EsHPC-300, EsHPC-350, EsHPC-400, EsHPC-450, EsHPC-500). Figure 6 shows the toluene adsorption penetration curves for ACs with corresponding calculated adsorption capacities listed in Table 5. Figure 6 exhibited a consistent S-shaped trend. These curves could be roughly categorized into three stages: Initially, the toluene concentration at the exit remained nearly constant at zero with no discernible increase; during the penetration stage, the toluene outlet concentration increased rapidly and approached the inlet concentration swiftly; finally, in the adsorption saturation stage, both inlet and outlet concentrations were very close, indicating that toluene adsorption by activated carbon was nearing saturation. The results of the toluene adsorption experiment indicated that, as the carbonization temperature increased from 300 to 500 °C, the toluene adsorption capacity of EhHPC and EsHPC initially increased and then decreased. Among ACs derived from EhHPR as the carbon precursor, EhHPC-300 exhibited the lowest toluene saturated adsorption capacity (576 $mg \cdot g^{-1}$), while EhHPC-400 demonstrated the highest toluene adsorption capacity at 816 $mg \cdot g^{-1}$. In contrast, for ACs produced derived from EsHPR as the carbon precursor, EsHPC-300 displayed the lowest toluene saturation adsorption capacity (585 $mg \cdot g^{-1}$), whereas EsHPC-400 showcased the highest toluene saturation capacity at 796 $mg \cdot g^{-1}$.

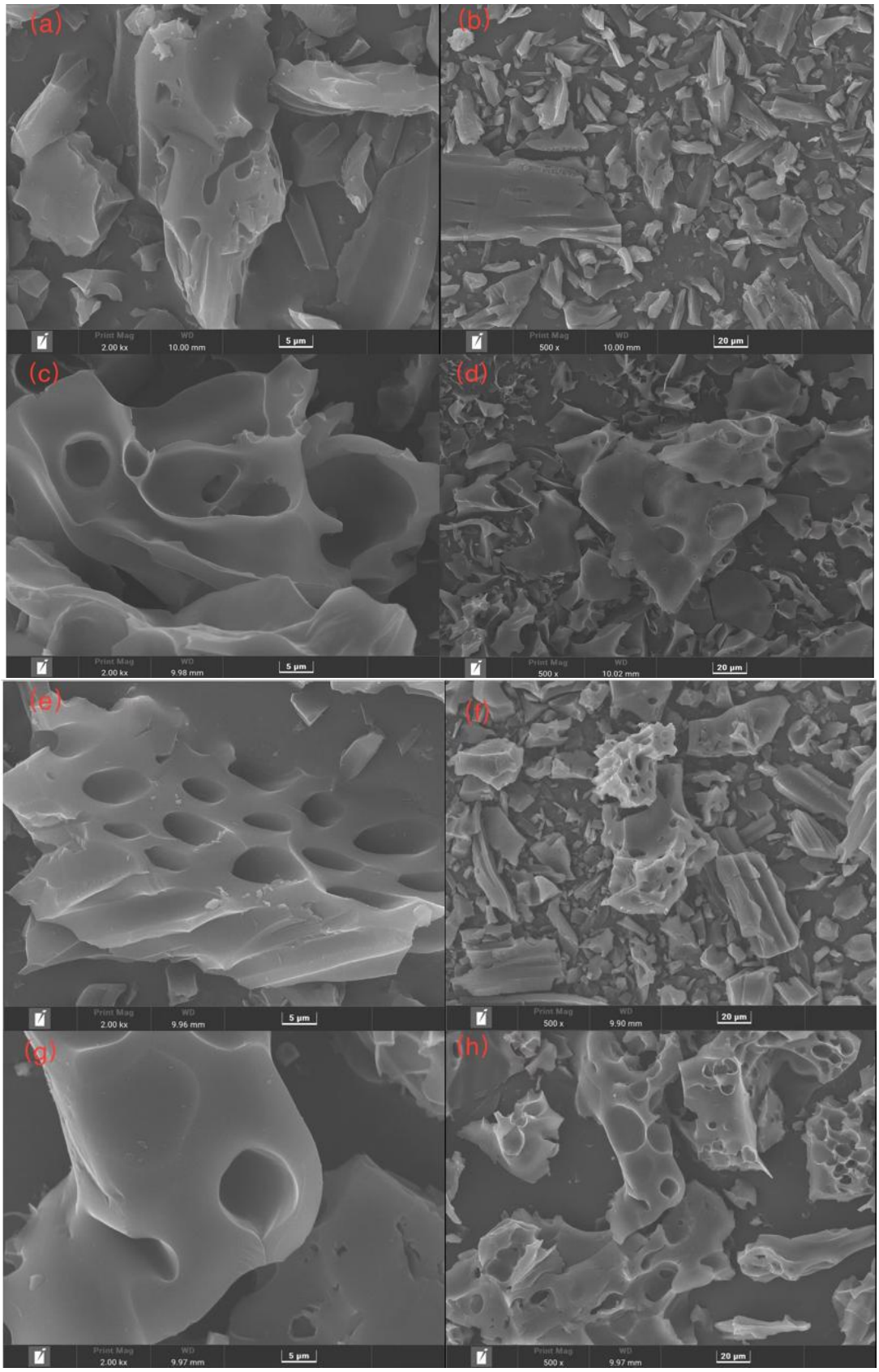

Fig. 5. SEM images of EhC-400(a, b), EsC-400(c, d), EhHPC-400(e, f) and EsHPC-400 (g, h)

The findings indicated that all the ACs prepared at carbonization temperatures ranging from 400 to 500 ℃ exhibited satisfactory adsorption capacity for toluene, with the best performance observed at 400 ℃. Additionally, the adsorption capacity of toluene experienced a significant increase between 300 and 400 ℃, which aligned with the variations in specific surface area and pore volume. The toluene adsorption penetration curves of EhHPC-400 and EsHPC-400 both lagged behind EhC-400 and EsC-400, indicating that the toluene adsorption capacity of ACs had been improved after the pre-extraction of hemicellulose.

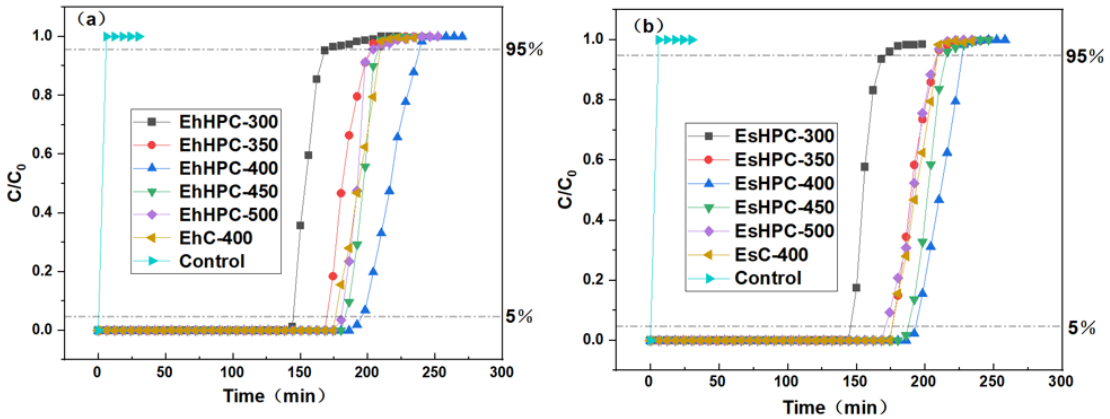

Fig. 6. Toluene adsorption penetration curves of ACs

Table 5. Adsorption Capacity of ACs for Toluene

Sample	Q_b (mg·g^{-1})	Q_s (mg·g^{-1})
EhC-400	637	694
EsC-400	642	702
EhHPC-300	533	576
EsHPC-300	540	585
EhHPC-350	598	647
EsHPC-350	589	642
EhHPC-400	768	816
EsHPC-400	750	796
EhHPC-450	675	723
EsHPC-450	713	764
EhHPC-500	646	698
EsHPC-500	635	683

The adsorption capacity of porous carbon material toluene is determined by its micropores (Lozano-Castello *et al.* 2002; Zhang *et al.* 2019a,b); micropores were the main adsorption sites. Mesoporous pores enhanced the diffusion within the particles and shortened the adsorption time (Zhang *et al.* 2017). As shown in Fig. 7, pore structure parameters S_{micro}, S_{meso}, V_{micro}, V_{meso} and toluene adsorption capacity were linearly fitted. The results indicated a strong linear correlation between the saturated adsorption capacity of toluene and S_{micro} and V_{micro} (R^2=0.9503, R^2=0.9313), suggesting that micropores played a dominant role in toluene adsorption on the ACs studied here. However, it was important to note that besides pore structure, various other factors also impacted the real adsorption process.

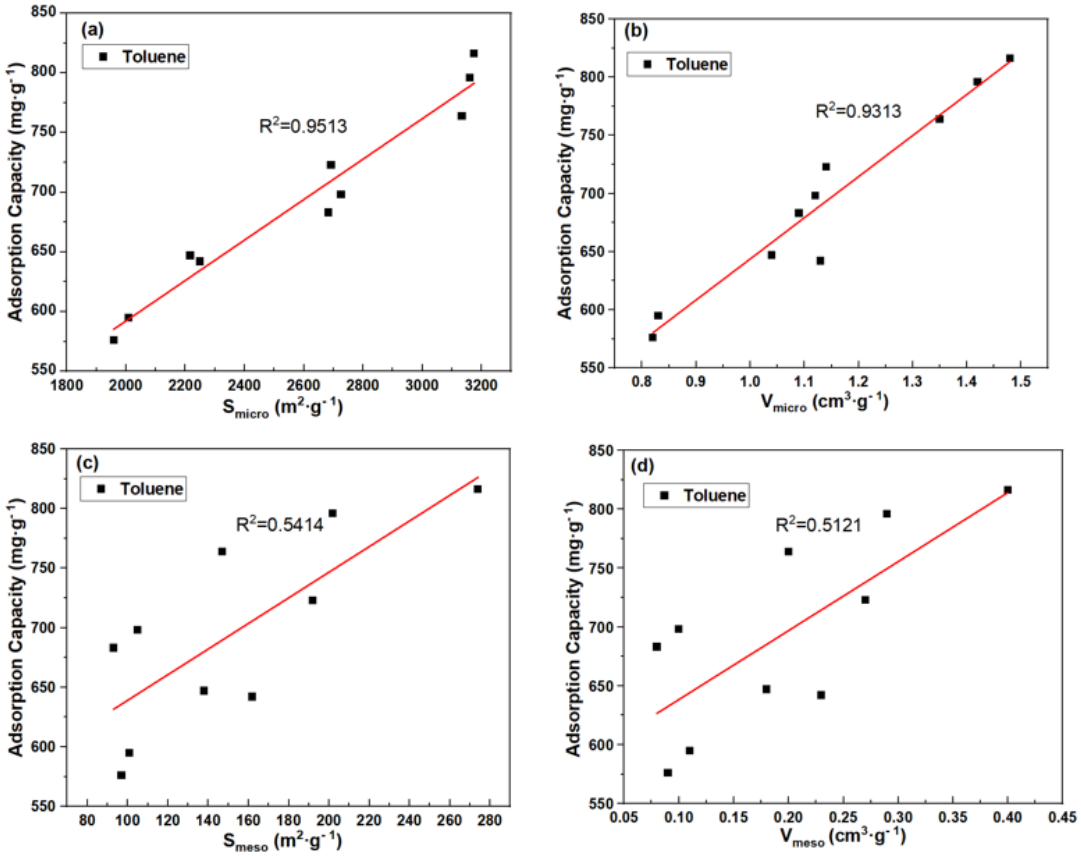

Fig. 7. The relationship between toluene adsorption capacity and pore structure parameters

Table 6 presents the toluene adsorption capacities of various other carbon materials, allowing for a comparison with the ACs prepared in this study. Compared with the ACs used in the laboratory chemical cabinets and the ACs reported in the literature, the ACs prepared in this work had a good adsorption capacity for toluene. EhHPC-400 demonstrated an exceptional toluene adsorption capacity of 816 mg·g^{-1}.

Table 6. Adsorption Capacity of Toluene on Different Carbon Materials

Sample	S_{BET} ($m^2 \cdot g^{-1}$)	Condition	Adsorption Capacity ($mg \cdot g^{-1}$)	Citations
EhHPC-400	3699	30 °C, 200 mL·min^{-1}, 500 ppm	816	This work
EsHPC-400	3553	30 °C, 200 mL·min^{-1}, 500 ppm	796	This work
$PK_{4\text{-}3}AC$	3066	30 °C, 100 mL·min^{-1}, 500 ppm	733	He *et al.* 2023
Commercial AC	885	30 °C, 100 mL ·min^{-1}, 500 ppm	295	From lab cabinet
HT180	1291	20 °C, 20 mL ·min^{-1}, 33803 mg·m^{-3}	533	Xie *et al.* 2022
CBAC-1.0-1.0 -550	1501	20 °C, 20 mL·min^{-1}, 33803 mg·m^{-3}	417	Zhu, *et al.* 2018
H3PO4-AC	3342	20 °C, 70 mL·min^{-} , *	506	Sessa *et al.* 2022
DBCB-AC	1213		580	Batur *et al.* 2022
DpAC58	1754		162	Isinkaralar 2022

•

This finding suggested that the appropriate carbonization temperature and the pre-extraction of hemicellulose enhanced the toluene adsorption performance of eucalyptus-

based activated carbon.

The fitting parameters of the Y-N model are shown in Table 6, and the correlation parameters R^2 were all over 0.96, indicating that the Y-N model could well predict the adsorption of toluene. Moreover, at carbonization temperatures ranging from 400 to 500 °C, K_{YN} (> 0.15), indicated favorable mass transfer performance.

Table 7. The Yoon-Nelson Model Fitting Parameters of EhHPC and EsHPC

Sample	K_{YN} (min^{-1})	T (min)	R^2
EhC-400	0.1531	184	0.9987
EsC-400	0.1544	185	0.9991
EhHPC-300	0.0901	154	0.9998
EsHPC-300	0.1115	155	0.9998
EhHPC-350	0.1450	182	0.9603
EsHPC-350	0.1271	188	0.9652
EhHPC-400	0. 1940	218	0.9658
EsHPC-400	0.1881	212	0.9655
EhHPC-450	0.1828	195	0.9788
EsHPC-450	0.1824	202	0.9728
EhHPC-500	0.1592	190	0.9648
EsHPC-500	0.1540	186	0.9789

CONCLUSIONS

1. Pre-extraction of hemicellulose from eucalyptus heartwood and sapwood with KOH at 85 °C degrees is not only beneficial to the high-value utilization of hemicellulose such as hydrogels, aerogels, drug carriers and sensors, but also to improve the pore characteristics and the toluene adsorption capacity of ACs prepared later. Following the pre-extraction of hemicellulose, the specific surface area of EhHPC-400 exhibited an increase of 986 $m^2 \cdot g^{-1}$, while the pore volume rose by 0.59 $cm^3 \cdot g^{-1}$ and the saturation capacity for toluene adsorption increased by 122 $mg \cdot g^{-1}$. In contrast, EsHPC-400 demonstrated a specific surface area enhancement of 690 $m^2 \cdot g^{-1}$, with a corresponding pore volume increase of 0.40 $cm^3 \cdot g^{-1}$ and an augmentation in toluene adsorption saturation capacity of 94 $mg \cdot g^{-1}$.
2. The carbonization temperature has a significant impact on the pore structure and distribution of activated carbon. An increase in carbonization temperature promotes pore expansion, facilitating the transformation from micropores to mesoporous pores and the generation of additional micropores. The optimized carbonization temperature is 400 °C. Excessively high carbonization temperatures, *i.e.*, increasing the carbonization temperature to 500 °C, may lead to some holes collapse and a reduction in specific surface area and pore volume of ACs.

3. The micropore content of activated carbon (< 2 nm) significantly influences the adsorption performance of toluene. The adsorption capacity of EhHPC-400 and EsHPC-400 for toluene was found to be 816 and 796 $mg \cdot g^{-1}$ respectively. Compared with the AC used in the laboratory chemical cabinets and the ACs reported in the literature, it was found that the ACs prepared in this study had better adsorption capacity of toluene.

REFERENCES CITED

Batur, E., and Kutluay, S. (2022). "Dynamic adsorption behavior of benzene, toluene, and xylene VOCs in single- and multi-component systems by activated carbon derived from defatted black cumin (*Nigella sativa* L.) biowaste," *Journal of Environmental Chemical Engineering* 10(3), article ID 107565. DOI: 10.1016/j.jece.2022.107565

David, E., and Niculescu, V. C. (2021). "Volatile organic compounds (VOCs) as environmental pollutants: Occurrence and mitigation using nanomaterials," *International Journal of Environmental Research and Public Health* 18(24), article ID 13147. DOI: 10.3390/ijerph182413147

GB/T 35818 (2018). "Standard method for analysis of forestry biomass – Determination of structural polysaccharides and lignin," Standardization Administration of China, Beijing, China.

GB/T 744 (2004). "Pulps – Determination of alkali resistance," Standardization Administration of China, Beijing, China.

Hassan, S. N., Ishak, M. A., and Ismail, K. (2014). "Co-liquefaction of rubber seed and low rank coal: Effect of weight ratio and temperature," *Environmental Science* 186, 511-518, article ID 110950976. DOI: 10.2495/ESUS140441

He, J., Zhao, Y., Zhou, Y., and Wu, S. (2023). "Preparation of high-performance activated carbons from hemicellulose pre-extracted residues of poplar and their application in VOCs removal," *BioResources* 18(2), 2874-2896. DOI: 10.15376/biores.18.2.2874-2896

Isinkaralar, K. (2022). "Theoretical removal study of gas BTEX onto activated carbon produced from *Digitalis purpurea* L. biomass," *Biomass Conversion and Biorefinery* 12(9), 4171-4181. DOI: 10.1007/s13399-022-02558-2

Li, P., Chen, T., Liu, M., Zheng, Y., Wei, Y., and Wu, W. (2024). "Preparation of grape branch-derived porous carbon by one-step blending and its multifunctional applications," *Diamond and Related Materials* 147, article 111331. DOI: 10.1016/j.diamond.2024.111331

Li, P., Yang, C., Yi, D., Li, S., Wang, M., Wang, H., Jin, Y., and Wu, W. (2023). "Preparation of spherical porous carbon from lignin-derived phenolic resin and its application in supercapacitor electrodes," *International Journal of Biological Macromolecules* 252, article 126271. DOI: 10.1016/j.ijbiomac.2023.126271

Li, Z., Li, Y. H., and Zhu, J. (2021). "Straw-based activated carbon: Optimization of the preparation procedure and performance of volatile organic compounds adsorption," *Materials* 14(12), article 3284. DOI: 10.3390/ma14123284

Lozano-Castello, D., Cazorla-Amoros, D., Linares-Solano, A., and Quinn, D. F. (2002). "Influence of pore size distribution on methane storage at relatively low pressure: Preparation of activated carbon with optimum pore size," *Carbon* 40(7), 989-1002.

DOI: 10.1016/S0008-6223(01)00235-4

Murata, K., Nakano, M., and Miyazaki, K. (2021). "Utilization of Chinese fast-growing trees and the effect of alternating lamination using mixed-species eucalyptus and poplar veneers," *J. Wood Sci.* 67(5). DOI: 10.1186/S10086-020-01937-5

Qin, P., Huang, D., Tang, R., Gan, F., and Lv, X. (2019). "Enhanced adsorption of sulfonamide antibiotics in water by modified biochar derived from bagasse," *Open Chemistry* 17(1), 1309-1316. DOI: 10.1515/chem-2019-0141

Sathya Priya, D., and Sureshkumar, M. V. (2019). "Synthesis of *Borassus flabellifer* fruit husk activated carbon filter for phenol removal from wastewater," *International Journal of Environmental Science and Technology* 17, 829-842. DOI: 10.1007/s13762-019-02325-3

Sessa, F., Merlin, G., and Canu, P. (2022). "Pine bark valorization by activated carbons production to be used as VOCs adsorbents," *Fuel* 318, article 123346. DOI: 10.1016/j.fuel.2022.123346

Wen, C., Liu, T., Wang, D., Wang, Y., Chen, H., Luo, G., Zhou, Z., Li, C., and Xu, M. (2023). "Biochar as the effective adsorbent to combustion gaseous pollutants: Preparation, activation, functionalization and the adsorption mechanisms," *Progress in Energy and Combustion Science* 99, article 101098. DOI: 10.1016/j.pecs.2023.101098

Wu, X., Lin, Y., Yi, Y., Wang, Y.-Y, Wu, S.-H, and Yang, C. (2023). "Volatile organic compound removal *via* biofiltration: Influences, challenges, and strategies," *Chemical Engineering Journal* 471, 144420.DOI: 10.1016/j.cej.2023.144420

Xie, L., Meng, Y., Wang, Q., Zhang, G. C., Xie, H., and Zhou, G. (2022). "*Zanthoxylum bungeanum* branches activated carbons with rich micropore structure prepared by low temperature H_3PO_4 hydrothermal pretreatment method for toluene adsorption," *Diamond and Related Materials* 130, 109474. DOI: 10.1016/j.diamond.2022.109474

Yang, F., Jin, C., Wang, S., Wang, Y., Wei, L., Zheng, L.H., Gu, H., Lam, S.S., Naushad, M., Li, C., and Sonne, C. (2023). "Bamboo-based magnetic activated carbon for efficient removal of sulfadiazine: Application and adsorption mechanism," *Chemosphere* 323, article 257174730. DOI: 10.1016/j.chemosphere.2023.138245

Yang, Q., Cui, P., Liu, C., Fang, G., Huang, M., Wang, Q., Zhou, Y., Hou, H., and Wang, Y. (2021). "*In situ* stabilization of the adsorbed Co^{2+} and Ni^{2+} in rice straw biochar based on LDH and its reutilization in the activation of peroxymonosulfate," *Journal of Hazardous Materials* 416, article 236246117. DOI: 10.1016/J.JHAZMAT.2021.126215

Yoon, Y. H., and Nelson, J. H. (1984). "Application of gas adsorption kinetics--II. A theoretical model for respirator cartridge service life and its practical applications," *American Industrial Hygiene Association Journal* 45(8), 517-524.

Zhang, X. Y., Gao, B., Creamer, A. E., Cao, C. C., and Li, Y. C. (2017). "Adsorption of VOCs onto engineered carbon materials: A review," *Journal of Hazardous Materials* 338, 102-123. DOI: 10.1016/j.jhazmat.2017.05.013

Zhang, W. X., Cheng, H. R., Niu, Q., Fu, M. L., Huang, H. M., and Ye, D. Q. (2019a). "Microbial targeted degradation pretreatment: A novel approach to preparation of activated carbon with specific hierarchical porous structures, high surface areas, and satisfactory toluene adsorption performance," *Environmental Science and Technology* 53(13), 7632-7640. DOI: 10.1021/acs.est.9b01159

Zhang, Z. K., Zhu, Z. Y., Shen, B. X., and Liu, L. N. (2019b). "Insights into biochar and

hydrochar production and applications: A review," *Energy* 171, 581-598. DOI: 10.1016/j.energy.2019.01.035

Zhu, J., Li, Y. H., Xu, L., and Liu, Z. Y. (2018). "Removal of toluene from waste gas by adsorption-desorption process using corncob-based activated carbons as adsorbents," *Ecotoxicology and Environmental Safety* 165, 115-125. DOI: 10.1016/j.ecoenv.2018.08.105

Zuo, Y., Feng, J., Soyol-Erdene, T., Wei, Z., Hu, T., Zhang, Y., and Tang, W. (2023). "Recent advances in wood-derived monolithic carbon materials: Synthesis approaches, modification methods and environmental applications," *Chemical Engineering Journal* 463, article 257479692. DOI: 10.1016/j.cej.2023.142332

Article submitted: October 23, 2024; Peer review completed: November 16, 2024; Revised version received: November 12, 2024; Accepted: December 10, 2024; Published: January 30, 2025.
DOI: 10.15376/biores.20.1.2259-2275